

# E-MD3C: Taming Masked Diffusion Transformers for Efficient Zero-Shot Object Customization

Trung X. Pham Zhang Kang Ji Woo Hong Xuran Zheng Chang D. Yoo  
KAIST  
School of Electrical Engineering

## Abstract

We propose E-MD3C (Efficient Masked Diffusion Transformer with Disentangled Conditions and Compact Collector), a highly efficient framework for zero-shot object image customization. Unlike prior works reliant on resource-intensive Unet architectures, our approach employs lightweight masked diffusion transformers operating on latent patches, offering significantly improved computational efficiency. The framework integrates three core components: (1) an efficient masked diffusion transformer for processing autoencoder latents, (2) a disentangled condition design that ensures compactness while preserving background alignment and fine details, and (3) a learnable Conditions Collector that consolidates multiple inputs into a compact representation for efficient denoising and learning. E-MD3C outperforms the existing approach on the VITON-HD dataset across metrics such as PSNR, FID, SSIM, and LPIPS, demonstrating clear advantages in parameters, memory efficiency, and inference speed. With only  $\frac{1}{4}$  of the parameters, our Transformer-based 468M model delivers  $2.5\times$  faster inference and uses  $\frac{2}{3}$  of the GPU memory compared to an 1720M Unet-based latent diffusion model.

## 1. Introduction

We address the challenge of zero-shot object-level image customization (ZSOIC) (Chen et al., 2024b), a task that has gained traction with the rise of diffusion models and open-source frameworks like Stable Diffusion (Rombach et al., 2022; Zhang et al., 2023). Existing methods, including ObjectStitch (Song et al., 2023) and Paint-by-Example (Yang et al., 2023), focus on localized edits but struggle with identity consistency, especially for unseen categories. Customization techniques such as Textual Inversion (Gal et al.,

\*Equal contribution. Correspondence to: Trung X. Pham <trungpx@kaist.ac.kr>, Chang D. Yoo <cd.yoo@kaist.ac.kr>.

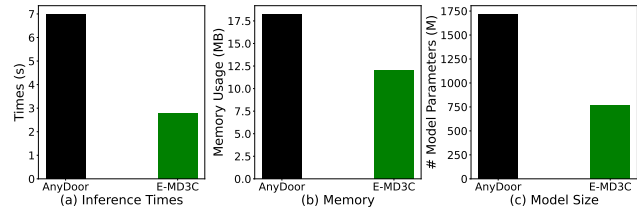


Figure 1: **Existing Approach Inefficiency.** The current model (black) demands significant parameters, memory, and inference time due to its resource-intensive architecture.

2022), DreamBooth (Ruiz et al., 2023), and UniCanvas (Jin et al., 2025) enable novel concept generation but lack spatial control and require extensive fine-tuning, limiting their real-world applicability. AnyDoor (Chen et al., 2024b) mitigates these issues by introducing a Stable Diffusion-based pipeline that ensures ID consistency in zero-shot settings, achieving flexible, high-quality region-specific edits using ID tokens and frequency-aware detail maps. However, its reliance on resource-heavy Unet-based architectures with ControlNet (Zhang et al., 2023) significantly increases computational overhead (see Fig. 1). Notably, prior works have largely overlooked the efficiency and potential of Vision Transformers (ViTs) (Dosovitskiy et al., 2021), which offer a compelling alternative to Unet-based designs. This raises a key question: *Can we achieve competitive performance while substantially reducing computational costs?*

Inspired by recent advances in transformer-based diffusion models, such as DiT (Peebles & Xie, 2023; Esser et al., 2024; Xie et al., 2025) and masked diffusion transformers (Gao et al., 2023; Pham et al., 2024; Mao et al., 2024; Pham et al., 2025), we explore their efficiency and adaptability for ZSOIC. Diffusion transformers (Peebles & Xie, 2023) offer stable training and strong generative performance, outperforming traditional Unet-based approaches (Ho et al., 2020; Rombach et al., 2022), making them well suited for this task. We introduce E-MD3C, a novel framework that employs masked diffusion transformers (Gao et al., 2023) for ZSOIC. Our approach features a specialized disentangled collection network that consolidates conditions into a compact vector for adaptive LayerNorm modulation, alongside a masking network to enhance transformer learning. Despite its simple

yet effective design, E-MD3C surpasses existing methods in FID, SSIM, L1, and LPIPS on the VITON-HD dataset (Choi et al., 2021), while significantly reducing parameter count and computational demands. Our main contributions are as follows:

- We propose E-MD3C, the first masked diffusion transformer-based model for zero-shot object customization, achieving high efficiency through latent patches and compact multi-condition representations.
- A novel Conditions Collector Module (CCM) is introduced to consolidate essential information into a lightweight representation for denoising diffusion, significantly reducing computational complexity compared to methods that concatenate full conditions with noisy target images.
- Our framework decouples conditions into two branches: the hint image supervises the target image in the denoising branch, while other conditions are processed via the CCM and a single cross-attention layer. This design enhances token alignment, preserves background details, and ensures robust correspondence between target and source images.
- E-MD3C outperforms the heavy Unet-based approach across multiple metrics, using only a quarter of the parameters and achieving  $2.5\times$  faster inference.

## 2. Related Works

**Zero-shot Object Customization.** Chen et al. (2024b) introduced AnyDoor to tackle the ZSOIC problem, utilizing a large pre-trained diffusion model, Stable Diffusion (Rom-bach et al., 2022), with a dual-backbone architecture inspired by ControlNet (Zhang et al., 2023). Despite achieving strong performance, AnyDoor relies on a resource-intensive architecture with significant computational demands, making the image generation process inefficient. Similarly, Chen et al. (2024a) proposed MimicBrush, a Unet-based latent diffusion model that integrates a reference U-Net into an imitative U-Net, offering finer part-level control but requiring a large model size and heavy computational resources. UniCanvas (Jin et al., 2025) also employs a substantial framework built upon customized text-to-image generation with Stable Diffusion, introducing a novel affordance-aware editing pipeline but further amplifying computational overhead with its parallel generative branches. While these approaches improve object customization applications, their reliance on oversized CNN-based architectures limits practical usage and applicability, especially on hardware with limited resources. To address these shortcomings, we propose E-MD3C, a lightweight transformer-based diffusion model that generates high-quality images while significantly reducing resource requirements (see Fig. 1).

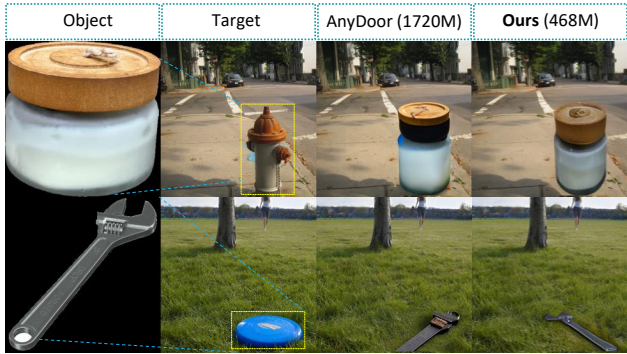


Figure 2: **Object Composition.** The 3<sup>rd</sup> and 4<sup>th</sup> columns show outputs from the existing method and our model. Our model generates images in just over 2 seconds, compared to 7 seconds for the existing approach.

**Denoising Diffusion Transformers.** The CNN-based U-Net architecture (Ronneberger et al., 2015) has long been the foundational framework for diffusion models and remains a prevalent choice for various diffusion-based generation tasks (Ho et al., 2020; 2022; Song & Ermon, 2019). However, a transformative shift occurred with the introduction of DiT (Peebles & Xie, 2023), which incorporated the transformer-based ViT architecture (Dosovitskiy et al., 2021) into latent diffusion models. This innovation demonstrated superior scalability and consistently outperformed traditional U-Net-based designs. Building on this progress, Gao et al. (2023) further advanced diffusion transformers, achieving state-of-the-art results in class-conditional image generation on ImageNet through advanced contextual representation learning. Other works, such as Stable Diffusion v3 (Esser et al., 2024), PixArt (Chen et al., 2025) and Sana (Xie et al., 2025), have leveraged DiT for text-to-image generation, highlighting the strong potential of transformer architectures in generative tasks. Although prior studies primarily focus on general-purpose or text-driven generative tasks, our research investigates the application of diffusion transformers to the specialized and complex task of zero-shot object-level image customization (ZSOIC). ZSOIC involves extracting and integrating intricate attributes from a source image, including object appearance, identity, and background, into a unified target image, which poses unique challenges in achieving cohesive synthesis (Ginesu et al., 2012; Chen et al., 2024b) (See Fig. 2).

**Mask Prediction Modeling.** Mask-based vision models, drawing inspiration from mask language models like BERT (Devlin et al., 2018), have demonstrated exceptional scalability and performance across diverse tasks. Prominent examples include MAE (He et al., 2022) for self-supervised learning (SSL) and models such as MaskGIT (Chang et al., 2022), Muse (Chang et al., 2023), and MAGVIT (Yu et al., 2023a), which learn discrete token distributions for image

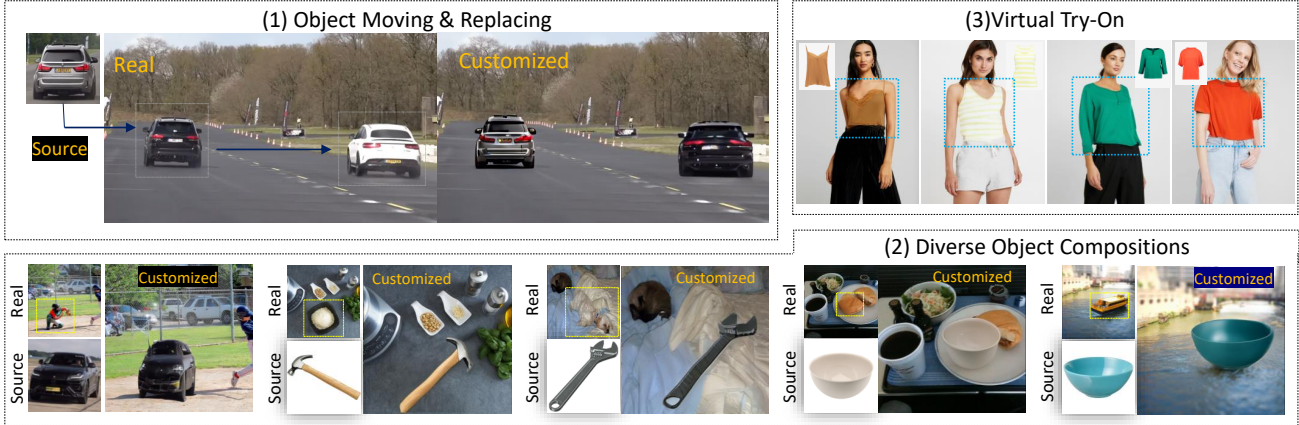


Figure 3: Zero-shot object customization and its practical applications. Images are generated using our E-MD3C model.

generation. These methods adopt non-autoregressive modeling with a cross-entropy loss to predict token indices within a codebook. Diverging from this paradigm, MDT (Gao et al., 2023) introduced an asymmetric masking schedule that enhances contextual representation learning in denoising diffusion transformers, achieving superior class-conditional image generation on ImageNet. Building on this foundation, Pham et al. (2024) proposed X-MDPT, demonstrating the potential of masked diffusion transformers for pose-guided human image generation with improved performance and efficiency. Similarly, MDT-A2G (Mao et al., 2024) applied masked diffusion transformers to gesture generation, while QA-MDT (Li et al., 2024) extended this framework for music generation. Further advancements include masked diffusion transformers for audio generation, as explored by MDSGen (Pham et al., 2025), achieving impressive results and inspiring subsequent research. In this work, we focus on leveraging the strengths of masked diffusion transformers (Gao et al., 2023) for the task of zero-shot object-level image customization, introducing E-MD3C, a disentangled design with multiple conditioning mechanisms to enable effective and targeted object generation with various applications as shown in Fig. 3.

### 3. Method

We propose a simple yet effective framework to tackle the ZSOIC task using diffusion transformers (Peebles & Xie, 2023). The overall architecture is illustrated in Fig. 4. Our method, E-MD3C, is composed of three core modules: (1) **Denoising Transformer-based Diffusion Network** (DTDNet): This serves as the backbone for generating high-quality target images through iterative denoising. (2) **Disentangled Masked Diffusion Module** (DMDNet): A novel masking-based design that models contextual relationships within the predicted target image by leveraging hints and noisy latents. This masking branch acts as a powerful regularization mechanism for the transformer, enhancing

its contextual learning ability. (3) **Learnable Conditions Collector** (CCNet): This module aggregates residual information from the source image and bounding box details into a compact vector, facilitating efficient denoising and improved learning performance. In the following sections, we delve into each component in detail.

#### 3.1. Denoising Transformer-based Diffusion Network

In our E-MD3C framework, this network component is referred to as DTDNet for brevity. Built on top of DiT (Peebles & Xie, 2023), DTDNet leverages a Transformer architecture to implement the diffusion process. For a  $512 \times 512$  resolution case, the framework operates as follows: Given a source image containing the desired object  $X_s \in \mathbb{R}^{512 \times 512 \times 3}$  and the target box position  $y_b$  within a hint image  $H \in \mathbb{R}^{512 \times 512 \times 3}$  (represented in the VAE latent space as  $h \in \mathbb{R}^{64 \times 64 \times 4}$ ), the goal is to learn the model parameters  $\theta$  to capture the target box, while preserving the style and content of the object from the source image, to generate the target image  $Y \in \mathbb{R}^{512 \times 512 \times 3}$ . To achieve this, we first utilize a pre-trained Stable Diffusion VAE (Rombach et al., 2022) to project the pixel-space images into latent representations  $x_s \in \mathbb{R}^{64 \times 64 \times 4}$  and  $y \in \mathbb{R}^{64 \times 64 \times 4}$ , facilitating efficient denoising. The denoising network  $\epsilon_\theta$ , a transformer-based diffusion model (Peebles & Xie, 2023), learns the conditional distribution  $p_\theta(y|x_s, y_b)$ . During training, Gaussian noise  $\epsilon \sim \mathcal{N}(0, \mathbf{I})$  is progressively added to the target image  $y$ , producing a noisy version  $y_t$  at each time step  $t \in [1, T]$ . The conditions—comprising  $x_s$ , the box  $y_b$ , and the hint  $h$ —are encapsulated in the conditional vector  $\vec{c}$ . The training objective is to predict the added noise by minimizing the mean squared error:

$$\mathcal{L}_{\text{denoising}} = \mathbb{E}_{y, \vec{c}, \epsilon \sim \mathcal{N}(0, \mathbf{I}), t} \|\epsilon - \epsilon_\theta(y_t, \vec{c}, t)\|^2. \quad (1)$$

After training  $p_\theta$ , the inference process starts with a random noise image  $y_T \sim \mathcal{N}(0, \mathbf{I})$ . The model then iteratively samples  $y_{t-1} \sim p_\theta(y_{t-1}|y_t)$  until it generates the

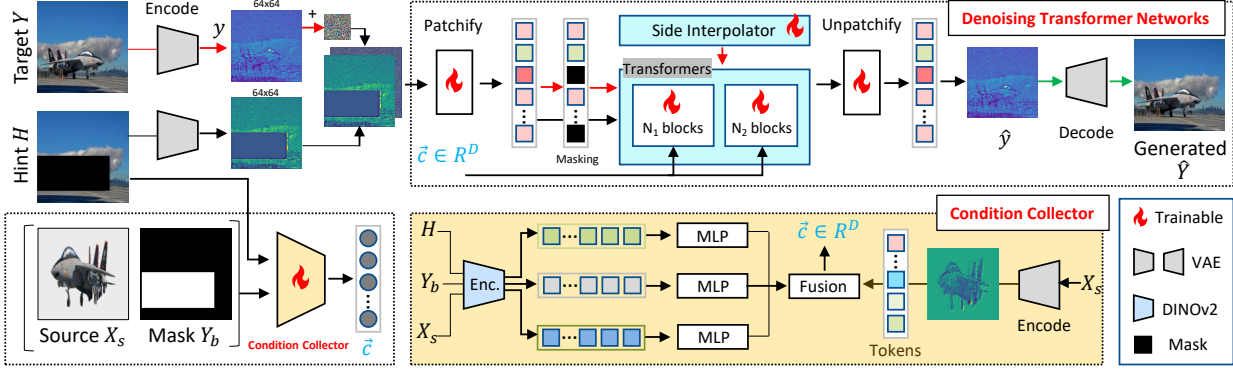


Figure 4: Overview of the E-MD3C framework for zero-shot object customization. During training, 30% of patched tokens are masked, and the noisy input is processed by the Diffusion Transformer, conditioned on a collected vector ( $D = 1024$ ) via AdaLN modulation (Peebles & Xie, 2023). A mask prediction objective models token relationships. The red arrow  $\rightarrow$  is training-only, the black arrow  $\rightarrow$  is used for both training and inference, and the green arrow  $\rightarrow$  is inference-only.

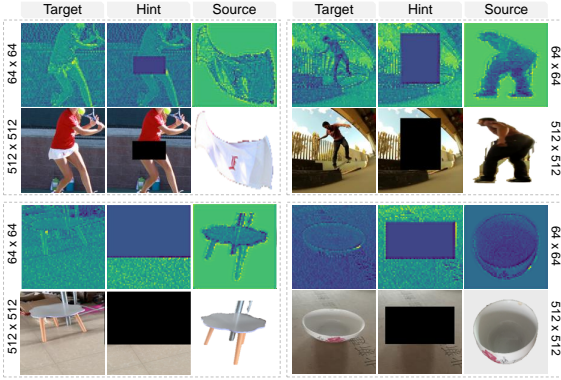


Figure 5: **Training data with diverse object sizes.** In the pixel space ( $512 \times 512$ ), objects of varying sizes and positions train the model, with black areas marking masked objects in bounding boxes. In the latent space ( $64 \times 64$ ), box position is preserved.

final target image  $y_0$ . Our diffusion transformer network is built upon the DiT architecture (Peebles & Xie, 2023). In this process, the noisy target latent  $y_t \in \mathbb{R}^{64 \times 64 \times 4}$  is concatenated with the hint latent  $h \in \mathbb{R}^{64 \times 64 \times 4}$  to produce  $y_{cat} \in \mathbb{R}^{64 \times 64 \times 8}$ . This combined latent is divided into patches of size  $p = 2$ , resulting in a sequence of patches  $z_{y_t} = [z_y^{(1)}, z_y^{(2)}, \dots, z_y^{(L_y)}] \in \mathbb{R}^{L_y \times D}$ , where  $L_y$  denotes the sequence length, and  $D$  is the embedding dimension. The conditional vector  $\vec{c}$  is integrated into DTDNet through adaptive layer normalization (AdaLN-Zero), following the default settings of the DiT framework. Fig. 5 illustrates examples of training data featuring objects of various sizes and perspectives, often derived from two random frames within a video, as described in (Chen et al., 2024b).

### 3.2. Conditions Collector Network (CCNet)

The Conditions Collector Network (CCNet) integrates four key inputs: (1) the target box condition feature (TBF), (2) the hint image feature (HIF) extracted from DINOv2, (3) the global source image feature (GSIF) derived from the

pre-trained DINOv2 model, and (4) the local source image feature obtained from the VAE. These inputs are processed to generate a compact conditional vector  $\vec{c}$ , matching the width of the Transformer ( $D = 1024$  in our model).

**Local Source Image Feature.** As discussed in (Pham et al., 2024), the local source image feature (LSIF) ensures alignment between the source image and the noisy target image within the DTDNet. This facilitates the transfer of crucial information such as appearance, texture, and identity from the source image to generate a harmonious object within the target box. Specifically, the source image latent ( $64 \times 64 \times 4$ ) is transformed into a sequence of patches  $z_{x_s} = [z_x^{(1)}, z_x^{(2)}, \dots, z_x^{(L_x)}] \in \mathbb{R}^{L_x \times D}$ , where  $L_x = 1024$ . This sequence serves as the local source image feature (LSIF =  $z_{x_s} \in \mathbb{R}^{1024 \times D}$ ).

**Masked Box Feature.** The masked box feature is derived from a 3-channel RGB visualization of the target box ( $224 \times 224 \times 3$ ), which serves as input to CCNet. We employ the pre-trained DINOv2-B model to extract features, generating a CLS token and 256 patch tokens that are concatenated into a sequence of 257 tokens (TBF  $\in \mathbb{R}^{257 \times D}$ ). This sequence is passed through a  $1 \times 1$  convolutional layer, reducing the 257 channels to a single channel, resulting in the vector  $v_B \in \mathbb{R}^D$ .

**Composed Global Source Image Feature.** To capture both the identity-preserving details of the object and the global context from the hint image, we extract DINO features from both the source and hint images. Previous works such as AnyDoor (Chen et al., 2024b) and X-MDPT (Pham et al., 2024) have demonstrated the effectiveness of self-supervised models like DINO in capturing fine-grained object details and identity. Using DINOv2-G, we extract the CLS token and concatenate it with 256 patch tokens to form the global features (GSIF1  $\in \mathbb{R}^{257 \times D}$  and GSIF2  $\in \mathbb{R}^{257 \times D}$  for the source and hint images, respectively). The input images, originally at  $512 \times 512$  resolution,

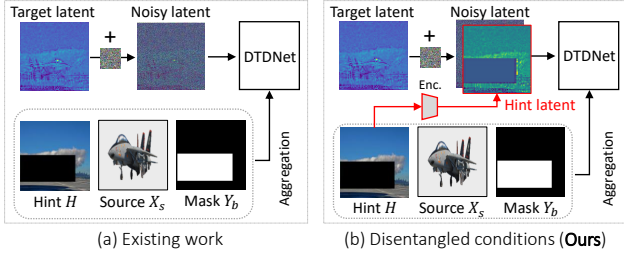


Figure 6: **Existing Design (Pham et al., 2024) vs. Ours.** Our approach leverages the VAE latent of the hint image to guide noisy target generation, enabling efficient adaptation to visible information outside the boxed region.

are resized to  $224 \times 224$  to comply with DINO’s requirements (ensuring both dimensions are divisible by 14). The extracted features GSIF1 and GSIF2 are then combined through a single MLP layer to produce the global source image feature  $GSIF \in \mathbb{R}^{514 \times D}$ .

**Compact Conditions Representation.** To generate the final conditional vector, we concatenate the extracted features (LSIF,  $v_B$ , GSIF1, and GSIF2) along the channel dimension to form  $m = 1539$  channels. An  $1 \times 1$  convolution operation  $\mathcal{C}$  (Fusion) is applied, producing a compact conditional vector  $\vec{c} = \mathcal{C}(\text{LSIF}, v_B, \text{GSIF1}, \text{GSIF2}) \in \mathbb{R}^D$ . While the hint image provides valuable contextual information for target image prediction, our experiments reveal that combining its VAE and DINO features with those of the source image is essential for accurate generation and faster model convergence. This compact vector significantly reduces the computational load and mitigates the risk of overfitting compared to methods like (Chen et al., 2024b), which process the full dimensions of all conditions alongside the noisy target image, leading to higher complexity.

### 3.3. Disentangled Masked Diffusion Module

Recently, Pham et al. (2024) adapted MDT (Gao et al., 2023), originally designed for class-conditional generation, to human image synthesis by modifying MDT to learn the distribution. Their method combines all conditions into a single vector, which is then used to modulate the noisy target image, achieving strong results in person image generation across various poses. However, for zero-shot object customization, this approach is ineffective (see Fig. 7), as the task aligns more closely with conditional inpainting. Here, the target image contains partial information that aids in predicting the missing regions, unlike generating an entire image purely from conditions. Fig. 6 illustrates the distinction between their design and our proposed solution, which we term “disentangled conditions.” Our approach separates the conditions into two distinct branches:

**Noisy Latent Processing Branch.** This branch leverages the VAE hint latent, which is pixel-aligned with the noisy

target latent  $y_t$ , to supervise the reconstruction of the visual information outside the masked region. This design reduces the model’s burden to only predicting the missing content within the bounding box. Specifically, we concatenate the hint latent and the noisy target latent along the channel dimension:

$$y_{\text{cat}}(t) = \text{concat}(h, y_t) \in \mathbb{R}^{64 \times 64 \times 8}. \quad (2)$$

The concatenated latent is then patchified using a patch size of  $p = 2$ , following the default configuration of DiT. Unlike previous methods (Peebles & Xie, 2023; Gao et al., 2023; Pham et al., 2024), which directly patchify the noisy target latent  $y_t$ , this step better incorporates contextual information.

**Condition Processing Branch.** The remaining conditions are processed similarly to Pham et al. (2024), yielding a lightweight vector that guides the denoising process. To enhance training, we introduce a masking mechanism in the latent space, randomly masking 30% of the patchified latent tokens, as in Gao et al. (2023). The loss function for training with masked tokens aligns with the standard denoising loss:

$$\mathcal{L}_{\text{denoising\_mask}} = \mathbb{E}_{y, \vec{c}, \epsilon \sim \mathcal{N}(0, \mathbf{I}), t} \|\epsilon - \epsilon_{\theta}(\mathcal{S}_{\theta}(x_s, y_m), \vec{c}, t)\|^2, \quad (3)$$

where  $\mathcal{S}_{\theta}$  is the network comprising  $N_1$  encoder layers, a side-interpolator, and  $N_2$  decoder layers, as defined in DTDNet. These components, along with other architectural settings, remain consistent with MDT (Gao et al., 2023). The side-interpolator (Gao et al., 2023) applies self-attention to learn contextual relationships among masked tokens, defined as:

$$\mathcal{S}_{\theta}(z_{y_m}) = z_{y_m} + \varphi_{\text{self-attention}}(z_{y_m}, z_{y_m}, z_{y_m}), \quad (4)$$

where  $\varphi_{\text{self-attention}}$  follows the attention mechanism proposed by Vaswani et al. (2017):

$$\varphi_{\text{self-attention}}(\mathbb{Q}, \mathbb{K}, \mathbb{V}) = \text{softmax}\left(\frac{\mathbb{Q}\mathbb{K}^{\top}}{\sqrt{d_k}}\right)\mathbb{V}. \quad (5)$$

**Final Objective Function.** The model jointly optimizes two loss functions:

$$\mathcal{L}_{\text{join}} = \mathcal{L}_{\text{denoising}} + \lambda \mathcal{L}_{\text{denoising\_mask}}, \quad (6)$$

where the masking branch with the side-interpolator acts as a strong regularizer during training but is omitted during inference, as introduced in MDT (Gao et al., 2023). This disentangled approach reduces computational complexity and mitigates overfitting, making it more effective for zero-shot object customization.  $\lambda$  is set to 1 as MDT’s default.

Table 1: Comparison of E-MD3C and existing methods on the VITON test set (Choi et al., 2021), using only bounding boxes without pose or segmentation masks, as required in virtual try-on tasks. All methods are trained on the same data under a zero-shot object customization setting. ‘\*’ indicates our design with disentangled conditions.

| Method                       | FID ↓       | PSNR ↑       | LPIPS ↓       | SSIM ↑        | L1 ↓            | Infer. Time (s) ↓ | #Params ↓   | External Data |
|------------------------------|-------------|--------------|---------------|---------------|-----------------|-------------------|-------------|---------------|
| X-MDPT (Pham et al., 2024)   | 13.70       | 15.75        | 0.2496        | 0.7051        | 8.19E-05        | 2.8 ± 0.02        | 468M        | ×             |
| DiT (Peebles & Xie, 2023)*   | 11.78       | 17.84        | 0.1865        | 0.7950        | 5.98E-05        | 2.8 ± 0.02        | 468M        | ×             |
| AnyDoor (Chen et al., 2024b) | 8.55        | 19.24        | 0.1730        | 0.7992        | 5.56E-05        | 7.1±0.05          | 1720M       | ✓             |
| <b>E-MD3C (Ours)</b>         | <b>8.47</b> | <b>19.38</b> | <b>0.1625</b> | <b>0.8106</b> | <b>4.92E-05</b> | <b>2.8 ± 0.02</b> | <b>468M</b> | ×             |

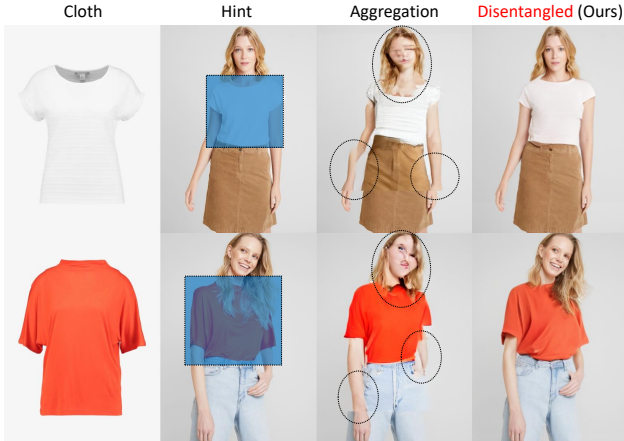


Figure 7: **Aggregation vs Disentangled Hinting.** Images are generated by methods on the VITON-HD dataset. Differences are shown more clearly in the face and hand regions. It is best viewed with zoom in at least 200%.

### 3.4. Dynamic Classifier-Free Guidance

We adopt dynamic classifier-free guidance (dy-CFG) (Ho & Salimans, 2022), following (Gao et al., 2023; Pham et al., 2024; 2025), where the predicted noise is computed as a weighted sum of the unconditional model  $\epsilon_\theta(y_t, t)$  and the conditional model  $\epsilon_\theta(y_t, \vec{c}, t)$ :

$$\hat{\epsilon}_\theta(y_t, x, t) = \beta_t \epsilon_\theta(y_t, \vec{c}, t) + (1 - \beta_t) \epsilon_\theta(y_t, t). \quad (7)$$

The guidance scale  $\beta_t$  varies dynamically at each timestep  $t$ . To CFG, we randomly set the conditional vector  $\vec{c} \in \mathbb{R}^D$ , obtained from CCNet, to a zero vector  $\vec{o} \in \mathbb{R}^D$  with a probability of  $\eta = 10\%$  during training. The guidance scale follows a power-cosine schedule:

$$\beta_t = \frac{1 - \cos \pi(\frac{t}{T})^\gamma}{2} \times \beta, \quad (8)$$

consistent with MDT (Gao et al., 2023). We use default values of  $\beta = 2.0$  and  $\gamma = 0.01$ .

## 4. Experiments

### 4.1. Implementation Details

**Dataset.** Our training dataset integrates multiple public datasets, including video and multi-view image datasets,

to extract source and target images. These are obtained from either two arbitrary video frames or two random object views. We utilize a subset of datasets from AnyDoor (Chen et al., 2024b), specifically YouTubeVOS, Saliency, VIPSeg, MVIImageNet, SAM, VITON-HD, Mose, FashionTryon, LVIS, and DressCode, excluding certain datasets due to difficulties in downloading or processing. For evaluation, we focus on high-resolution images from the VITON-HD test set (Choi et al., 2021) at  $512 \times 512$  resolution. Preprocessing follows prior work (Chen et al., 2024b), with source object images and segmentation masks used DINOv2 (Oquab et al., 2023) at  $224 \times 224$  input size, while the source object image maintains  $512 \times 512$  resolution for input into the VAE.

**Metrics.** We adopt standard evaluation metrics from prior research (Choi et al., 2021; Bhunia et al., 2023; Pham et al., 2024), including FID, PSNR, SSIM, LPIPS, and L1, utilizing evaluation scripts provided by DisCo (Wang et al., 2024). Our approach is benchmarked against the primary baseline, AnyDoor (Chen et al., 2024b), replacing their resource-intensive double Stable Diffusion backbone with our efficient Transformer-based model while maintaining consistent dataset processing for fair comparison. Additionally, for object composition tasks lacking ground truth, we follow prior works by using CLIP and DINO scores to evaluate performance.

**Training.** We use the pre-trained VAE with ft-MSE from Stable Diffusion. For  $512 \times 512$  images, training was conducted on a single A100 GPU with a batch size 5 for 1.5 million steps. For ablation studies, we trained the model for 300k steps. The learning rate was set to  $1 \times 10^{-4}$ , with an EMA rate of 0.9999, and other settings were consistent with those in DiT (Peebles & Xie, 2023; Pham et al., 2024).

Table 2: **Objects Composition.** Results are presented for image generation at  $512 \times 512$  resolution on our collected data and DreamBooth (Ruiz et al., 2023) test set.

| Method                       | CLIP <sub>score</sub> ↑ | DINO <sub>score</sub> ↑ | External Data |
|------------------------------|-------------------------|-------------------------|---------------|
| AnyDoor (Chen et al., 2024b) | 0.7306                  | <b>0.4831</b>           | ✓             |
| <b>E-MD3C (Ours)</b>         | <b>0.7322</b>           | 0.4702                  | ×             |

### 4.2. Main Results

**Quantitative Results.** Tab. 1 presents a comparative evaluation of various methods for the **virtual try-on task**, where

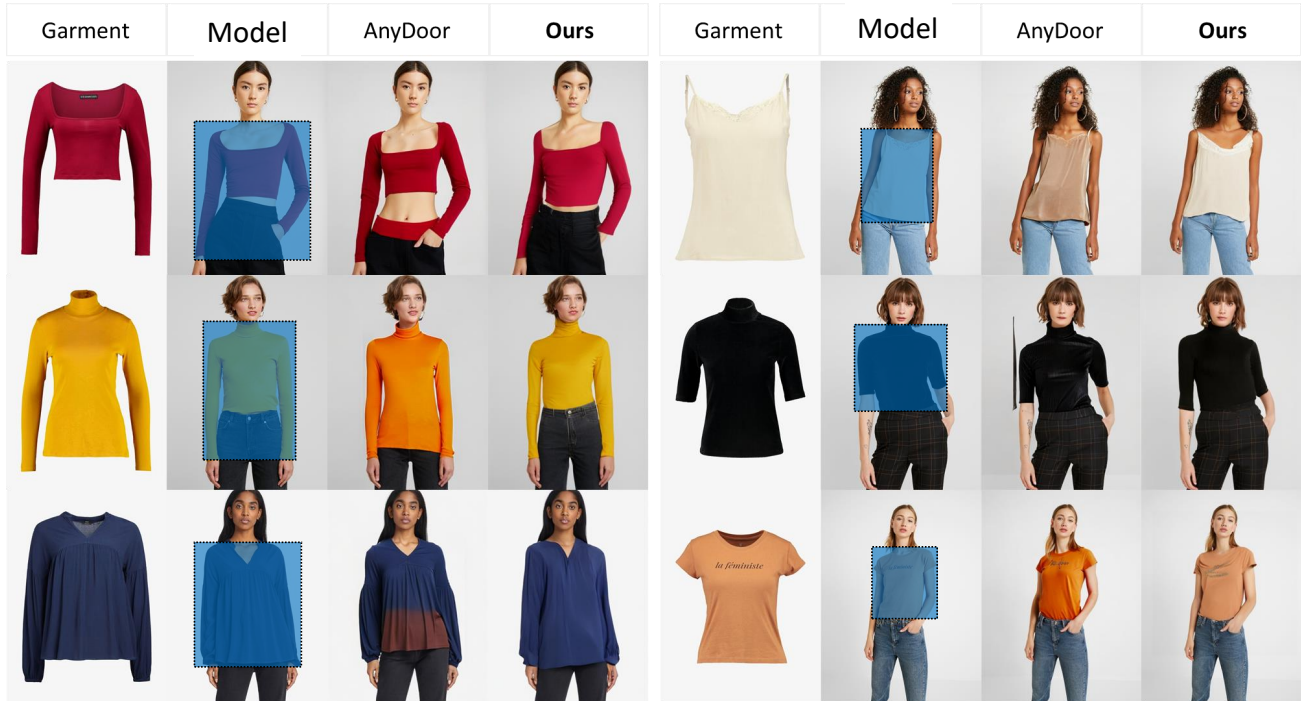


Figure 8: **Qualitative Comparison.** Results on the VITON-HD dataset demonstrate the performance of various approaches. Given two inputs – a cloth image and a model hint image with a boxed region indicating where to place the cloth—our transformer-based E-MD3C (468M) effectively handles diverse scenarios, producing more realistic and ground truth-aligned outputs compared to the CNN-based method AnyDoor (Chen et al., 2024b).

models operate without pose estimation or segmentation masks, relying only on a clothing item and a rough bounding box. Our E-MD3C consistently outperforms others across FID, SSIM, LPIPS, and L1 metrics at a resolution of  $512 \times 512$ . Unlike AnyDoor (Chen et al., 2024b), which depends on a large-scale model pretrained on billions of text-image pairs from the LAION dataset, our method achieves strong results without such extensive pretraining, highlighting its efficiency. **For object composition** (Tab. 2), our method performs comparably to AnyDoor in CLIP scores and slightly lags in DINO scores, likely due to AnyDoor’s backbone being trained on a broader set of objects, including those in DreamBooth datasets. However, the performance gap is small and can be bridged with additional video training data, which is readily available. Given the significantly lower computational demands of our approach, E-MD3C presents a far more practical and scalable solution.

**Qualitative Results.** Fig. 8 compares the outputs of E-MD3C with those of existing methods. Our approach consistently produces high-quality try-on images across various scenarios. In contrast, the Unet-based AnyDoor (Chen et al., 2024b), built on a heavy double-Unet ControlNet (Zhang et al., 2023) architecture, often struggles to capture fine-grained clothing details, leading to noticeable artifacts. By leveraging latent-space processing and a transformer with masked modeling for semantic understanding, E-MD3C ac-

curately preserves intricate garment details, resulting in more realistic and visually coherent images. Additional qualitative results are available in the **Appendix**.

### 4.3. Ablation Studies

For ablation studies, we evaluate high-resolution VITON-HD (Choi et al., 2021) test images, analyzing metrics and the impact of different configurations. Visual comparisons further illustrate the effectiveness of each modification.

#### 4.3.1. IMPACT OF DECOUPLED CONDITIONS

As shown in Fig. 9, using only the hint image in the denoising branch alongside the noisy target image fails to achieve optimal convergence. Decoupling the hint image features with DINO and processing them separately in the CCNet condition branch significantly accelerates training and enhances generation accuracy.

#### 4.3.2. COMPARED EFFICIENCY

We quantitatively demonstrate the efficiency and speed advantages of our method over AnyDoor (Chen et al., 2024b), as shown in Tab. 3. AnyDoor relies on a large, 1720M parameter model that requires 7.1 seconds and 18GB of GPU memory per image generation. In contrast, our lightweight



Figure 9: **Generated images with different training steps.** Adding DINO features of hint image showing a better convergence. It is best viewed with zoom in 200%.

468M parameter model achieves the same task in just 2.8 seconds while using only 12GB of memory. This significant reduction in both inference time and memory usage highlights the practicality of our Transformer-based framework, especially when compared to the Unet-based Stable Diffusion and the resource-intensive ControlNet-style methods. These results emphasize our method’s superior efficiency, making it more practical for real-world applications where computational resources and time are often limited.

Table 3: **Compare Efficiency.** Results are presented for a single image generation (batch size  $B = 1$ ) for  $512 \times 512$  resolution, 50 DDIM denoising steps, using one NVIDIA A100 GPU. We conduct 10 runs and take the average.

| Method           | Infer. Time $\downarrow$ | Mem. (M) $\downarrow$ | #Param. $\downarrow$ | Type   |
|------------------|--------------------------|-----------------------|----------------------|--------|
| AnyDoor [CVPR24] | $7.0 \pm 0.05s$          | 18273                 | 1720M                | Unet   |
| E-MD3C (Ours)    | $2.8 \pm 0.02s$          | 12071                 | 468M                 | Trans. |

#### 4.3.3. HINT IMAGE AS SUPERVISION

Fig. 7 highlights the limitations of the aggregation-based approach (Pham et al., 2024), which fails in zero-shot object customization. Unlike pose-guided person generation, where source and target images share similar structures, target images in object customization often contain unseen parts and backgrounds. This emphasizes the need for a more flexible, disentangled condition representation.

#### 4.3.4. IMPACT OF MASKING MODELING

We analyze the impact of masking learning on the zero-shot object customization task, particularly in multiview learning. By examining how the learnable vector from CCNet correlates with different views in the MVImageNet (Yu et al., 2023b) test set, we find that DiT (Peebles & Xie, 2023) struggles to maintain view consistency without masking modeling (see Fig. 10). In contrast, our method with masking learning achieves significantly higher similarity across views, demonstrating that it effectively captures key object features and remains robust across various perspectives.

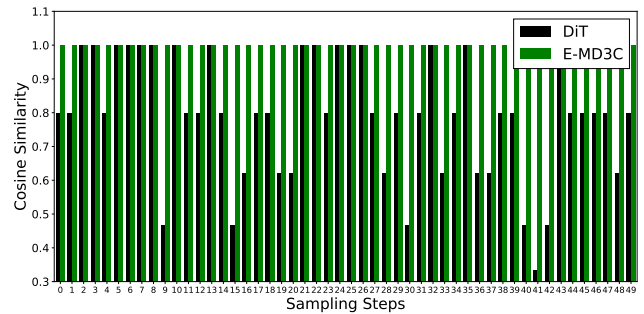


Figure 10: Conditional alignment of various source object image views. Our transformer-based E-MD3C model achieves superior alignment scores, measured via cosine similarity, compared to baseline foundation models.

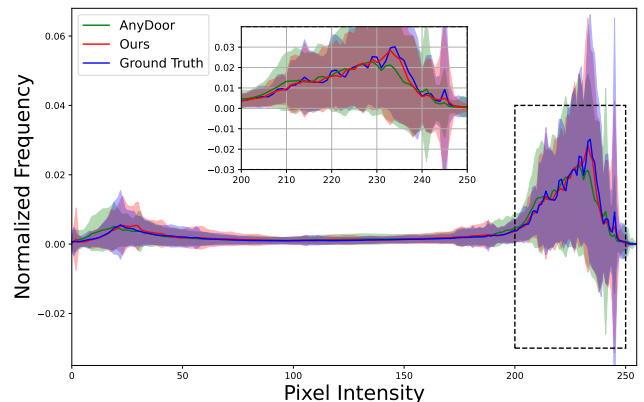


Figure 11: **Pixel Distribution.** Compare generated images and ground truth (GT). Our method aligns more closely with the GT curve, while AnyDoor (Chen et al., 2024b) exhibits noticeable deviations. Best viewed at 200% zoom.

#### 4.3.5. DISTRIBUTION STATISTIC

To compare the behavior of our model with existing methods, we compute the pixel statistics of the outputs generated by both approaches on the VITON-HD dataset. As shown in Fig. 11, our method produces a pixel distribution that aligns more closely with the ground truth compared to the AnyDoor model. This suggests that the Transformer-based diffusion model captures the data distribution more effectively than the Unet-based model.

## 5. Conclusion

In this paper, we present E-MD3C, a novel masked diffusion generative model tailored for zero-shot object customization (ZSOIC). Unlike previous methods that rely on resource-heavy Unet-based backbones for denoising diffusion, our approach utilizes a masked diffusion transformer architecture operating on latent patches, significantly improving efficiency. Extensive experiments demonstrate that E-MD3C not only produces high-quality, high-resolution images but also achieves faster inference speeds, highlighting its potential as an effective and efficient solution for this task.

## Impact Statement

Our method effectively generates high-quality images across various object customization tasks, offering a flexible virtual try-on solution with just a simple bounding box. It provides significant advantages, including faster image generation compared to existing large, slow models. However, as with all image synthesis technologies, there is a potential for misuse, such as creating deceptive content. We are committed to implementing safeguards to regulate access, ensuring the technology benefits the community while minimizing risks.

## References

- Athar, A., Luiten, J., Voigtlaender, P., Khurana, T., Dave, A., Leibe, B., and Ramanan, D. Burst: A benchmark for unifying object recognition, segmentation and tracking in video. In *Proceedings of the IEEE/CVF winter conference on applications of computer vision*, pp. 1674–1683, 2023.
- Bhunia, A. K., Khan, S., Cholakkal, H., Anwer, R. M., Laaksonen, J., Shah, M., and Khan, F. S. Person image synthesis via denoising diffusion model. In *Proceedings of the IEEE/CVF Conference on Computer Vision and Pattern Recognition*, pp. 5968–5976, 2023.
- Borji, A., Cheng, M.-M., Jiang, H., and Li, J. Salient object detection: A benchmark. *IEEE transactions on image processing*, 24(12):5706–5722, 2015.
- Chang, H., Zhang, H., Jiang, L., Liu, C., and Freeman, W. T. Maskgit: Masked generative image transformer. In *Proceedings of the IEEE/CVF Conference on Computer Vision and Pattern Recognition*, pp. 11315–11325, 2022.
- Chang, H., Zhang, H., Barber, J., Maschinot, A., Lezama, J., Jiang, L., Yang, M.-H., Murphy, K., Freeman, W. T., Rubinstein, M., et al. Muse: Text-to-image generation via masked generative transformers. *arXiv preprint arXiv:2301.00704*, 2023.
- Chen, J., Ge, C., Xie, E., Wu, Y., Yao, L., Ren, X., Wang, Z., Luo, P., Lu, H., and Li, Z. Pixart: Weak-to-strong training of diffusion transformer for 4k text-to-image generation. In *European Conference on Computer Vision*, pp. 74–91. Springer, 2025.
- Chen, X., Feng, Y., Chen, M., Wang, Y., Zhang, S., Liu, Y., Shen, Y., and Zhao, H. Zero-shot image editing with reference imitation. In *The Thirty-eighth Annual Conference on Neural Information Processing Systems*, 2024a. URL <https://openreview.net/forum?id=LZV0U6UHb6>.
- Chen, X., Huang, L., Liu, Y., Shen, Y., Zhao, D., and Zhao, H. Anydoor: Zero-shot object-level image customization. In *Proceedings of the IEEE/CVF Conference on Computer Vision and Pattern Recognition*, pp. 6593–6602, 2024b.
- Choi, S., Park, S., Lee, M., and Choo, J. Viton-hd: High-resolution virtual try-on via misalignment-aware normalization. In *Proceedings of the IEEE/CVF conference on computer vision and pattern recognition*, pp. 14131–14140, 2021.
- Cong, W., Zhang, J., Niu, L., Liu, L., Ling, Z., Li, W., and Zhang, L. Dovenet: Deep image harmonization via domain verification. In *Proceedings of the IEEE/CVF conference on computer vision and pattern recognition*, pp. 8394–8403, 2020.
- Devlin, J., Chang, M.-W., Lee, K., and Toutanova, K. Bert: Pre-training of deep bidirectional transformers for language understanding. *arXiv preprint arXiv:1810.04805*, 2018.
- Ding, H., Liu, C., He, S., Jiang, X., Torr, P. H., and Bai, S. Mose: A new dataset for video object segmentation in complex scenes. In *Proceedings of the IEEE/CVF International Conference on Computer Vision*, pp. 20224–20234, 2023.
- Dosovitskiy, A., Beyer, L., Kolesnikov, A., Weissenborn, D., Zhai, X., Unterthiner, T., Dehghani, M., Minderer, M., Heigold, G., Gelly, S., et al. An image is worth 16x16 words: Transformers for image recognition at scale. *arXiv preprint arXiv:2010.11929*, 2010.
- Dosovitskiy, A., Beyer, L., Kolesnikov, A., Weissenborn, D., Zhai, X., Unterthiner, T., Dehghani, M., Minderer, M., Heigold, G., Gelly, S., Uszkoreit, J., and Houlsby, N. An image is worth 16x16 words: Transformers for image recognition at scale. In *ICLR*, 2021.
- Esser, P., Kulal, S., Blattmann, A., Entezari, R., Müller, J., Saini, H., Levi, Y., Lorenz, D., Sauer, A., Boesel, F., et al. Scaling rectified flow transformers for high-resolution image synthesis. In *Forty-first International Conference on Machine Learning*, 2024.
- Gal, R., Alaluf, Y., Atzmon, Y., Patashnik, O., Bermano, A. H., Chechik, G., and Cohen-Or, D. An image is worth one word: Personalizing text-to-image generation using textual inversion. *arXiv preprint arXiv:2208.01618*, 2022.
- Gao, S., Zhou, P., Cheng, M.-M., and Yan, S. Masked diffusion transformer is a strong image synthesizer. In *Proceedings of the IEEE/CVF International Conference on Computer Vision*, pp. 23164–23173, 2023.
- Ginesu, G., Pintus, M., and Giusto, D. D. Objective assessment of the webp image coding algorithm. *Signal Processing: Image Communication*, 2012.

- Gupta, A., Dollar, P., and Girshick, R. Lvis: A dataset for large vocabulary instance segmentation. In *Proceedings of the IEEE/CVF conference on computer vision and pattern recognition*, pp. 5356–5364, 2019.
- He, K., Chen, X., Xie, S., Li, Y., Dollár, P., and Girshick, R. Masked autoencoders are scalable vision learners. In *Proceedings of the IEEE/CVF conference on computer vision and pattern recognition*, pp. 16000–16009, 2022.
- Ho, J. and Salimans, T. Classifier-free diffusion guidance. *arXiv preprint arXiv:2207.12598*, 2022.
- Ho, J., Jain, A., and Abbeel, P. Denoising diffusion probabilistic models. *Advances in neural information processing systems*, 33:6840–6851, 2020.
- Ho, J., Saharia, C., Chan, W., Fleet, D. J., Norouzi, M., and Salimans, T. Cascaded diffusion models for high fidelity image generation. *The Journal of Machine Learning Research*, 23(1):2249–2281, 2022.
- Jin, J., Shen, Y., Zhao, X., Fu, Z., and Yang, J. Unicanvas: Affordance-aware unified real image editing via customized text-to-image generation. *International Journal of Computer Vision*, pp. 1–25, 2025.
- Jung, Y. H., Hong, S. K., Wang, H. S., Han, J. H., Pham, T. X., Park, H., Kim, J., Kang, S., Yoo, C. D., and Lee, K. J. Flexible piezoelectric acoustic sensors and machine learning for speech processing. *Advanced Materials*, 32(35):1904020, 2020.
- Jung, Y. H., Pham, T. X., Issa, D., Wang, H. S., Lee, J. H., Chung, M., Lee, B.-Y., Kim, G., Yoo, C. D., and Lee, K. J. Deep learning-based noise robust flexible piezoelectric acoustic sensors for speech processing. *Nano Energy*, 101:107610, 2022.
- Kim, J., Ma, M., Pham, T., Kim, K., and Yoo, C. D. Modality shifting attention network for multi-modal video question answering. In *Proceedings of the IEEE/CVF conference on computer vision and pattern recognition*, pp. 10106–10115, 2020.
- Kirillov, A., Mintun, E., Ravi, N., Mao, H., Rolland, C., Gustafson, L., Xiao, T., Whitehead, S., Berg, A. C., Lo, W.-Y., et al. Segment anything. In *Proceedings of the IEEE/CVF International Conference on Computer Vision*, pp. 4015–4026, 2023.
- Lee, D., Park, H., Pham, T., and Yoo, C. D. Learning augmentation network via influence functions. In *Proceedings of the IEEE/CVF Conference on Computer Vision and Pattern Recognition*, pp. 10961–10970, 2020.
- Li, C., Wang, R., Liu, L., Du, J., Sun, Y., Guo, Z., Zhang, Z., and Jiang, Y. Quality-aware masked diffusion transformer for enhanced music generation. *arXiv preprint arXiv:2405.15863*, 2024.
- Mao, X., Jiang, Z., Wang, Q., Fu, C., Zhang, J., Wu, J., Wang, Y., Wang, C., Li, W., and Chi, M. Mdt-a2g: Exploring masked diffusion transformers for co-speech gesture generation. *arXiv preprint arXiv:2408.03312*, 2024.
- Miao, J., Wang, X., Wu, Y., Li, W., Zhang, X., Wei, Y., and Yang, Y. Large-scale video panoptic segmentation in the wild: A benchmark. In *Proceedings of the IEEE/CVF Conference on Computer Vision and Pattern Recognition*, pp. 21033–21043, 2022.
- Niu, A., Zhang, K., Pham, T. X., Sun, J., Zhu, Y., Kweon, I. S., and Zhang, Y. Cdpmsr: Conditional diffusion probabilistic models for single image super-resolution. In *2023 IEEE International Conference on Image Processing (ICIP)*, pp. 615–619. IEEE, 2023.
- Niu, A., Pham, T. X., Zhang, K., Sun, J., Zhu, Y., Yan, Q., Kweon, I. S., and Zhang, Y. Acddmsr: Accelerated conditional diffusion models for single image super-resolution. *IEEE Transactions on Broadcasting*, 2024a.
- Niu, A., Zhang, K., Pham, T. X., Wang, P., Sun, J., Kweon, I. S., and Zhang, Y. Learning from multi-perception features for real-word image super-resolution. *IEEE Transactions on Circuits and Systems for Video Technology*, 2024b.
- Oquab, M., Darcet, T., Moutakanni, T., Vo, H. V., Szafraniec, M., Khalidov, V., Fernandez, P., Haziza, D., Massa, F., El-Nouby, A., Howes, R., Huang, P.-Y., Xu, H., Sharma, V., Li, S.-W., Galuba, W., Rabbat, M., Assran, M., Ballas, N., Synnaeve, G., Misra, I., Jegou, H., Mairal, J., Labatut, P., Joulin, A., and Bojanowski, P. Dinov2: Learning robust visual features without supervision, 2023.
- Peebles, W. and Xie, S. Scalable diffusion models with transformers. In *Proceedings of the IEEE/CVF International Conference on Computer Vision*, pp. 4195–4205, 2023.
- Pham, T., Zhang, C., Niu, A., Zhang, K., and Yoo, C. D. On the pros and cons of momentum encoder in self-supervised visual representation learning. *arXiv preprint arXiv:2208.05744*, 2022a.
- Pham, T. X., Mina, R. J. L., Issa, D., and Yoo, C. D. Self-supervised learning with local attention-aware feature. *arXiv preprint arXiv:2108.00475*, 2021.

- Pham, T. X., Mina, R. J. L., Nguyen, T., Madjid, S. R., Choi, J., and Yoo, C. D. Lad: A hybrid deep learning system for benign paroxysmal positional vertigo disorders diagnostic. *IEEE Access*, 2022b.
- Pham, T. X., Niu, A., Zhang, K., Jin, T. J. T., Hong, J. W., and Yoo, C. D. Self-supervised visual representation learning via residual momentum. *IEEE Access*, 2023.
- Pham, T. X., Zhang, K., and Yoo, C. D. Cross-view masked diffusion transformers for person image synthesis. In *Forty-first International Conference on Machine Learning*, 2024.
- Pham, T. X., Ton, T., and Yoo, C. D. MDSGen: Fast and efficient masked diffusion temporal-aware transformers for open-domain sound generation. In *International Conference on Learning Representations*, 2025. URL <https://openreview.net/forum?id=yFEqYwgttJ>.
- Rombach, R., Blattmann, A., Lorenz, D., Esser, P., and Ommer, B. High-resolution image synthesis with latent diffusion models. In *Proceedings of the IEEE/CVF conference on computer vision and pattern recognition*, pp. 10684–10695, 2022.
- Ronneberger, O., Fischer, P., and Brox, T. U-net: Convolutional networks for biomedical image segmentation. In *International Conference on Medical image computing and computer-assisted intervention*, 2015.
- Ruiz, N., Li, Y., Jampani, V., Pritch, Y., Rubinstein, M., and Aberman, K. Dreambooth: Fine tuning text-to-image diffusion models for subject-driven generation. In *Proceedings of the IEEE/CVF conference on computer vision and pattern recognition*, pp. 22500–22510, 2023.
- Song, J., Meng, C., and Ermon, S. Denoising diffusion implicit models. *arXiv preprint arXiv:2010.02502*, 2020.
- Song, Y. and Ermon, S. Generative modeling by estimating gradients of the data distribution. *Advances in neural information processing systems*, 32, 2019.
- Song, Y., Zhang, Z., Lin, Z., Cohen, S., Price, B., Zhang, J., Kim, S. Y., and Aliaga, D. Objectstitch: Object compositing with diffusion model. In *Proceedings of the IEEE/CVF Conference on Computer Vision and Pattern Recognition*, pp. 18310–18319, 2023.
- Trung, P. X. and Yoo, C. D. Short convolutional neural network and mfccs for accurate speaker recognition systems. *International Technical Conference on Circuits/Systems, Computers and Communications (ITC-CSCC)*, 2019.
- Vaswani, A., Shazeer, N., Parmar, N., Uszkoreit, J., Jones, L., Gomez, A. N., Kaiser, L., and Polosukhin, I. Attention is all you need. In *NeurIPS*, 2017.
- Vu, T., Jang, H., Pham, T. X., and Yoo, C. Cascade rpn: Delving into high-quality region proposal network with adaptive convolution. *Advances in neural information processing systems*, 32, 2019.
- Wang, L., Lu, H., Wang, Y., Feng, M., Wang, D., Yin, B., and Ruan, X. Learning to detect salient objects with image-level supervision. In *Proceedings of the IEEE conference on computer vision and pattern recognition*, pp. 136–145, 2017.
- Wang, T., Li, L., Lin, K., Zhai, Y., Lin, C.-C., Yang, Z., Zhang, H., Liu, Z., and Wang, L. Disco: Disentangled control for realistic human dance generation. In *Proceedings of the IEEE/CVF Conference on Computer Vision and Pattern Recognition*, pp. 9326–9336, 2024.
- Wang, W., Feiszli, M., Wang, H., and Tran, D. Unidentified video objects: A benchmark for dense, open-world segmentation. In *Proceedings of the IEEE/CVF international conference on computer vision*, pp. 10776–10785, 2021.
- Xie, E., Chen, J., Chen, J., Cai, H., Tang, H., Lin, Y., Zhang, Z., Li, M., Zhu, L., Lu, Y., et al. SANA: Efficient high-resolution text-to-image synthesis with linear diffusion transformers. In *The Thirteenth International Conference on Learning Representations*, 2025. URL <https://openreview.net/forum?id=N80jlXhtYZ>.
- Xu, N., Yang, L., Fan, Y., Yue, D., Liang, Y., Yang, J., and Huang, T. Youtube-vos: A large-scale video object segmentation benchmark. *arXiv preprint arXiv:1809.03327*, 2018.
- Yang, B., Gu, S., Zhang, B., Zhang, T., Chen, X., Sun, X., Chen, D., and Wen, F. Paint by example: Exemplar-based image editing with diffusion models. In *Proceedings of the IEEE/CVF Conference on Computer Vision and Pattern Recognition*, pp. 18381–18391, 2023.
- Yang, L., Fan, Y., and Xu, N. Video instance segmentation. In *Proceedings of the IEEE/CVF international conference on computer vision*, pp. 5188–5197, 2019.
- Yu, L., Cheng, Y., Sohn, K., Lezama, J., Zhang, H., Chang, H., Hauptmann, A. G., Yang, M.-H., Hao, Y., Essa, I., et al. Magvit: Masked generative video transformer. In *Proceedings of the IEEE/CVF Conference on Computer Vision and Pattern Recognition*, pp. 10459–10469, 2023a.
- Yu, X., Xu, M., Zhang, Y., Liu, H., Ye, C., Wu, Y., Yan, Z., Zhu, C., Xiong, Z., Liang, T., et al. Mvimnet: A large-scale dataset of multi-view images. In *Proceedings of the IEEE/CVF conference on computer vision and pattern recognition*, pp. 9150–9161, 2023b.

Zhang, C., Zhang, K., Pham, T. X., Niu, A., Qiao, Z., Yoo, C. D., and Kweon, I. S. Dual temperature helps contrastive learning without many negative samples: Towards understanding and simplifying moco. In *Proceedings of the IEEE/CVF Conference on Computer Vision and Pattern Recognition*, pp. 14441–14450, 2022a.

Zhang, C., Zhang, K., Zhang, C., Pham, T. X., Yoo, C. D., and Kweon, I. S. How does simsiam avoid collapse without negative samples? a unified understanding with self-supervised contrastive learning. In *International Conference on Learning Representations*, 2022b. URL <https://openreview.net/forum?id=bwq6O4Cwdl>.

Zhang, L., Rao, A., and Agrawala, M. Adding conditional control to text-to-image diffusion models, 2023.

Zheng, N., Song, X., Chen, Z., Hu, L., Cao, D., and Nie, L. Virtually trying on new clothing with arbitrary poses. In *Proceedings of the 27th ACM international conference on multimedia*, pp. 266–274, 2019.

## A. Appendix

### A.1. More details of experimental setups

We use 50 steps DDIM (Song et al., 2020) for inference which is the same as AnyDoor (Chen et al., 2024b). The details of our method’s configuration are provided in Tab. 4. For VAE, we used the VAE of Stable Diffusion (Rombach et al., 2022).

Table 4: **Parameters and Configs.** We follow ViT (Dosovitskiy et al., 2010) to name models Large (L).

| Method | Layers | Dim. | Heads | Param. (M) | Method | Layers | Dim. | Heads | Param. (M) | Method | Layers | Dim. | Heads | Param. (M) |
|--------|--------|------|-------|------------|--------|--------|------|-------|------------|--------|--------|------|-------|------------|
| DiT-L  | 24     | 1024 | 16    | 458.0      | MDT-L  | 24     | 1024 | 16    | 459.1      | E-MD3C | 24     | 1024 | 16    | 468.0      |

### A.2. Datasets Used for Training

We utilize publicly available datasets, comprising a mix of image and video datasets, similar to AnyDoor (Chen et al., 2024b). However, due to challenges in downloading and processing, some datasets could not be included (‘×’ as denoted in the table). The datasets used for training our model are detailed in Tab. 5.

Table 5: **Training Dataset.** All datasets marked in ‘✓’ are used for training our model within the column “Ours Used”.

| Dataset                              | Type             | # Samples | Variation | Quality | AnyDoor Used | Ours Used |
|--------------------------------------|------------------|-----------|-----------|---------|--------------|-----------|
| YouTubeVOS (Xu et al., 2018)         | Video            | 4,450     | ✓         | Low     | ✓            | ✓         |
| YouTubeVIS (Yang et al., 2019)       | Video            | 2,883     | ✓         | Low     | ✓            | ×         |
| UVO (Wang et al., 2021)              | Video            | 10,337    | ✓         | Low     | ✓            | ×         |
| MOSE (Ding et al., 2023)             | Video            | 1,507     | ✓         | High    | ✓            | ✓         |
| VIPSeg (Miao et al., 2022)           | Video            | 3,110     | ✓         | High    | ✓            | ✓         |
| BURST (Athar et al., 2023)           | Video            | 1,493     | ✓         | Low     | ✓            | ×         |
| MVImgNet (Yu et al., 2023b)          | Multi-view Image | 104,261   | ✓         | High    | ✓            | ✓         |
| VITON-HD (Choi et al., 2021)         | Multi-view Image | 11,647    | ✓         | High    | ✓            | ✓         |
| FashionTryon (Zheng et al., 2019)    | Multi-view Image | 21,197    | ✓         | High    | ✓            | ✓         |
| MSRA (Borji et al., 2015)            | Single Image     | 10,000    | ×         | High    | ✓            | ✓         |
| DUT (Wang et al., 2017)              | Single Image     | 15,572    | ×         | High    | ✓            | ✓         |
| Flickr (Cong et al., 2020)           | Single Image     | 4,833     | ×         | High    | ✓            | ✓         |
| LVIS (Gupta et al., 2019)            | Single Image     | 117,287   | ×         | High    | ✓            | ✓         |
| SAM (subset) (Kirillov et al., 2023) | Single Image     | 100,864   | ×         | High    | ✓            | ✓         |

### A.3. Self-Supervised Learning Models

There are various SSL models have been explored to learn the representations without labels (He et al., 2022; Pham et al., 2021; 2023; Oquab et al., 2023; Zhang et al., 2022a;b). These models serve as a good extractor for various applications (Pham et al., 2022b; Chen et al., 2024b). DINOv2 (Oquab et al., 2023) demonstrated an excellent pre-trained model for various diffusion-based frameworks. We mainly use DINOv2, but the other options may be worth trying. With the potential of diffusion transformers for conditional learning, it is expected to have more discovery of its capability in various domains and applications such as speech processing (Jung et al., 2022; 2020; Trung & Yoo, 2019), data augmentation (Lee et al., 2020), VQA (Kim et al., 2020), visual detection learning (Vu et al., 2019), super-resolution (Niu et al., 2023; 2024a;b).

### A.4. More Quantitative Results

We demonstrate the effectiveness of our method in various object composition tasks, as illustrated in Fig. 12, Fig. 13, and Fig. 14.



Figure 12: **Object Composition.** Compared existing work AnyDoor and ours E-MD3C (1).

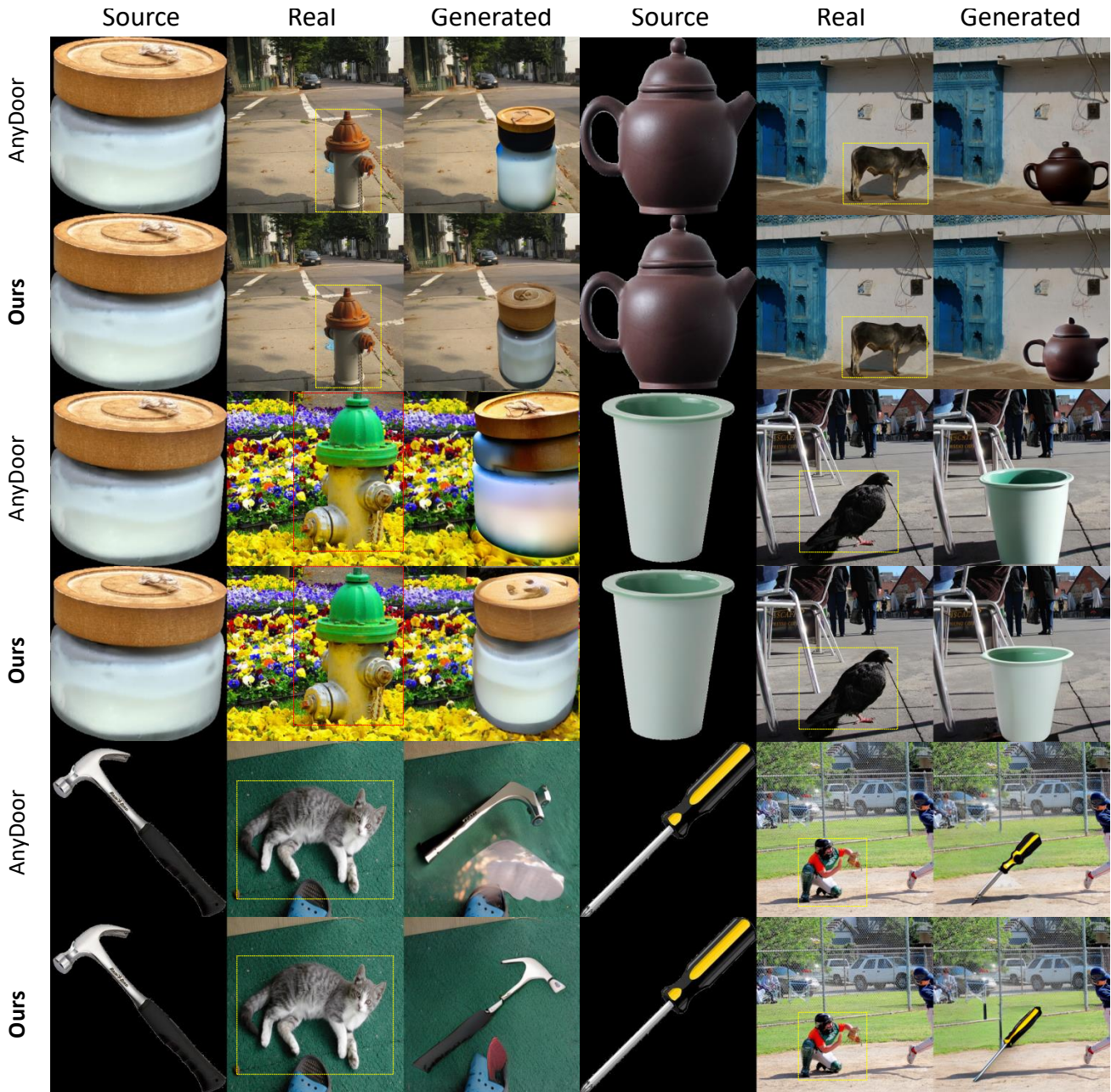


Figure 13: **Object Composition.** Compared existing work AnyDoor and ours E-MD3C (2).



Figure 14: **Object Composition.** Compared existing work AnyDoor and ours E-MD3C (3).